NASA-CR-167459

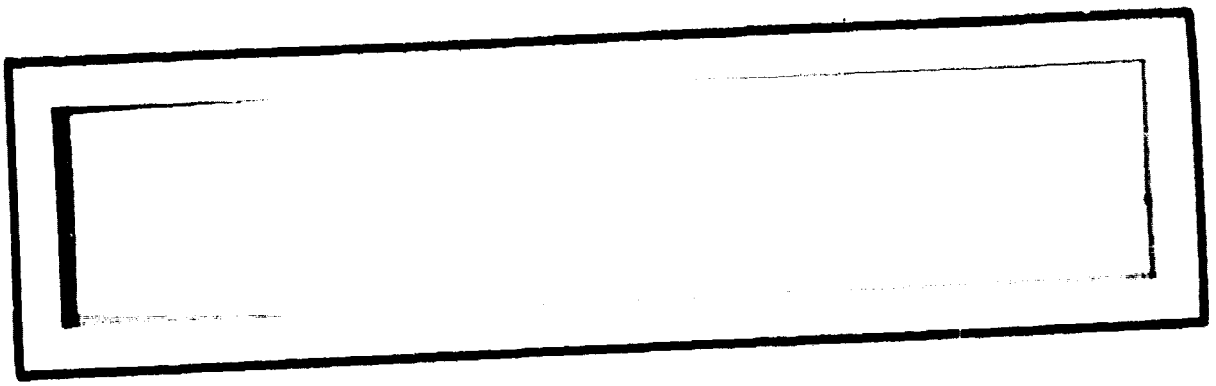

Axiomatix

(NASA-CR-167459) ENGINEERING EVALUATIONS AND STUDIES. REPORT FOR IUS STUDIES Final Annual Report, 1981 (Axiomatix, Los Angeles, Calif.) 44 p HC A03/MF A01 CSCL 22B

N82-15114

Unclas
G3/16 02651

NASA CR-167459

1. W.E. Teasdale EE8

2. ENGINEERING EVALUATIONS AND STUDIES
ANNUAL FINAL REPORT FOR IUS STUDIES

5. Contract No. NAS 9-16067, Exhibit A

Prepared for

Lyndon B. Johnson Space Center
Houston, Texas 77058

Prepared by

4. Axiomatix
9841 Airport Blvd., Suite 912
Los Angeles, California 90045

7. Axiomatix Report No. R8110-3
6. October 20, 1981

TABLE OF CONTENTS

1.0 INTRODUCTION

1.1 Statement of Work

1.1.1 Objectives

The objectives of this contract were to identify and resolve problems associated with the Orbiter/IUS communications systems.

1.1.2 Stipulated Tasks

The tasks associated with this contract include participation in design reviews, coupled with acceptance of action items to be undertaken for the resolution of review item dispositions (RID's). This includes reviewing all performance analyses submitted by the transponder contractor.

2.0 GENERAL APPROACH

In the process of carrying out the required tasks, Axiomatix has worked closely with the cognizant NASA personnel, the Orbiter prime contractor (Rockwell International), the IUS prime contractor (Boeing Aerospace Co.), and the IUS and Orbiter payload communication equipment subcontractor (TRW Defense and Space Group). This activity included attending the Critical Design Review (CDR) and reviewing in detail all communication-related performance analyses submitted by TRW.

While Axiomatix was engaged in these contractual activities, TRW, the IUS STDN/TDRS transponder contractor, received a stop-work order since the Centaur is to be used as an upper stage for NASA missions, and the NASA TDRS/GSTDN standard transponder built by Motorola was chosen for use on the Centaur. Therefore, the remainder of this report documented the analyses and investigations undertaken by Axiomatix and completed at the time of the stop-work order.

3.0 TECHNICAL INVESTIGATION

This section documents the reviews, investigations and analyses of the TRW IUS STDN/TDRS transponder performed by Axiomatix. First, it is appropriate to discuss where this equipment or subsystem fits into the overall Orbiter/Payload communication link. Figure 1 shows the top-level IUS STDN/TDRS transponder interfaces with the payload IUS and the Orbiter. As can be seen in this figure, the transponder receives telemetry from the IUS and passes commands to the IUS. The interface with the Orbiter is via an S-band RF link with the Payload Interrogator (PI). Thus, the IUS STDN/TDRSS transponder must perform all the typical communication functions of acquisition, tracking, data demodulation and data modulation. These functions will be addressed in subsequent sections.

Before analyzing these communication functions, however, it is helpful to gain some perspective as to where and how these functions relate to the overall transponder. This perspective is afforded by the transponder block diagram shown in Figure 2. The specific detailed areas of the transponder involved in the Axiomatix investigation are indicated by the cross-hatch lines in the transponder block diagram given in Figure 3.

3.1 Analysis of IUS STDN/TDRS Transponder Performance

Volume I (Analysis) of the STDN/TDRS Transponder, S-Band Critical Design Review (CDR) data package contains a series of detailed electrical design analyses performed by TRW for Boeing that pertain to the manner in which the STDN/TDRS transponder meets the performance specifications imposed by NASA for its use in IUS missions. Many of these analyses previously appeared in the Preliminary Design Review (PDR) data package delivered to Boeing on June 11, 1979. To the extent that these analyses (IUS memos) were complete at that time, Axiomatix reviewed and critiqued their contents and reported its findings shortly thereafter in Axiomatix Report No. R7911-5, November 30, 1979. Also included in that report were three appendices (C, E and F) which augmented and, in some instances, corrected several of the TRW analyses.

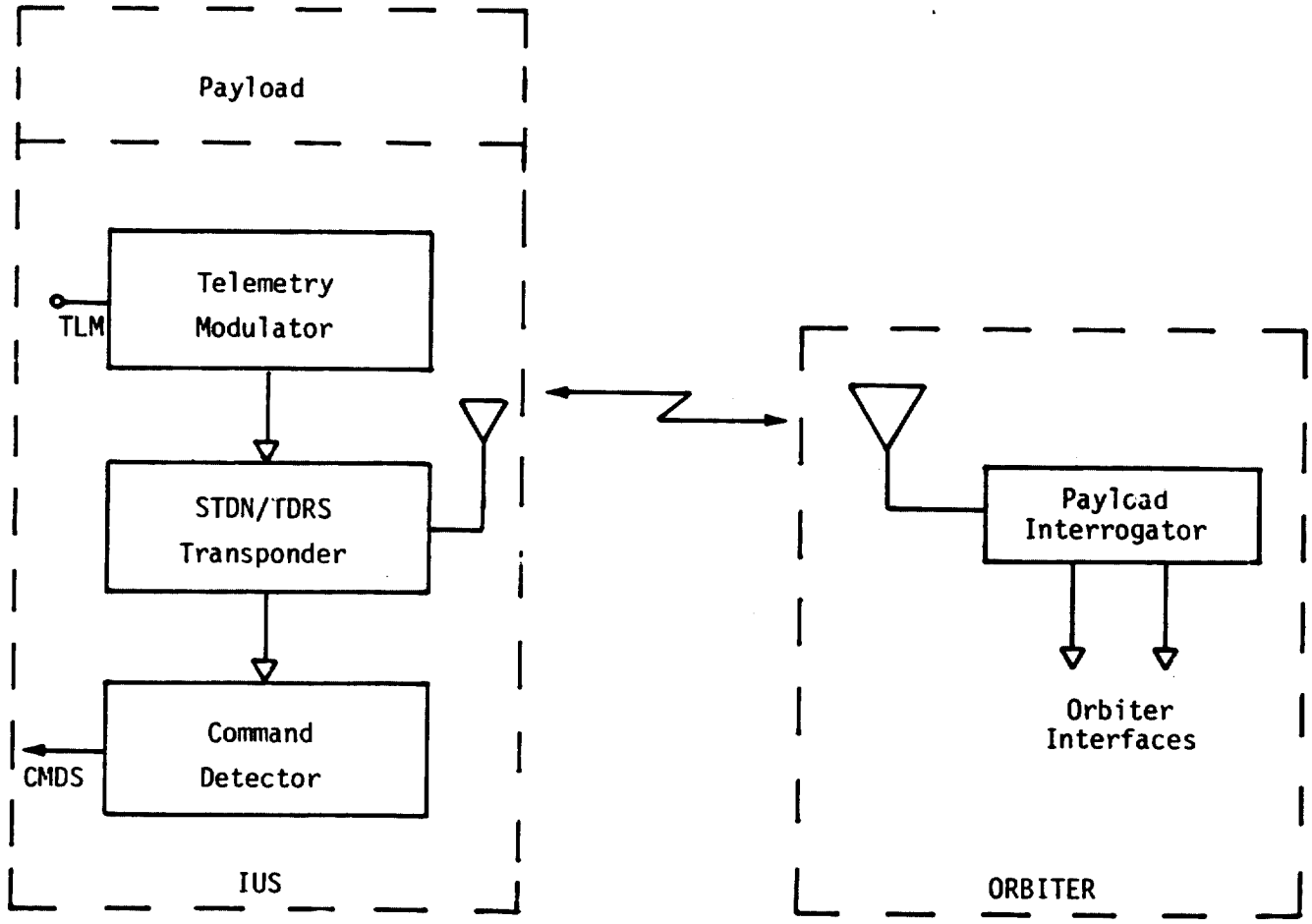

Figure 1. Top-Level IUS STDN/TDRS Transponder Interfaces

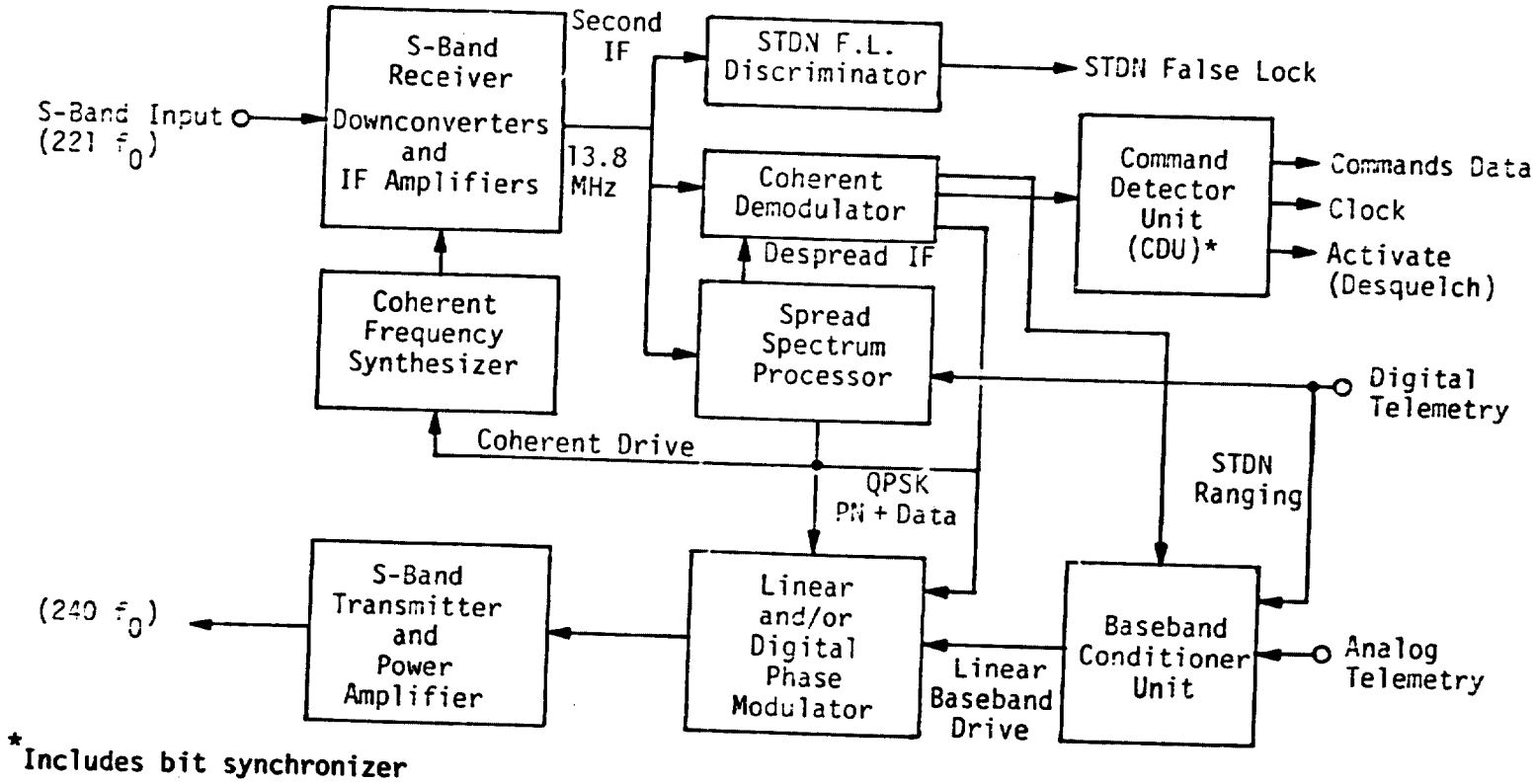

Figure 2. IUS STDN/TDRS Transponder Functional Block Diagram

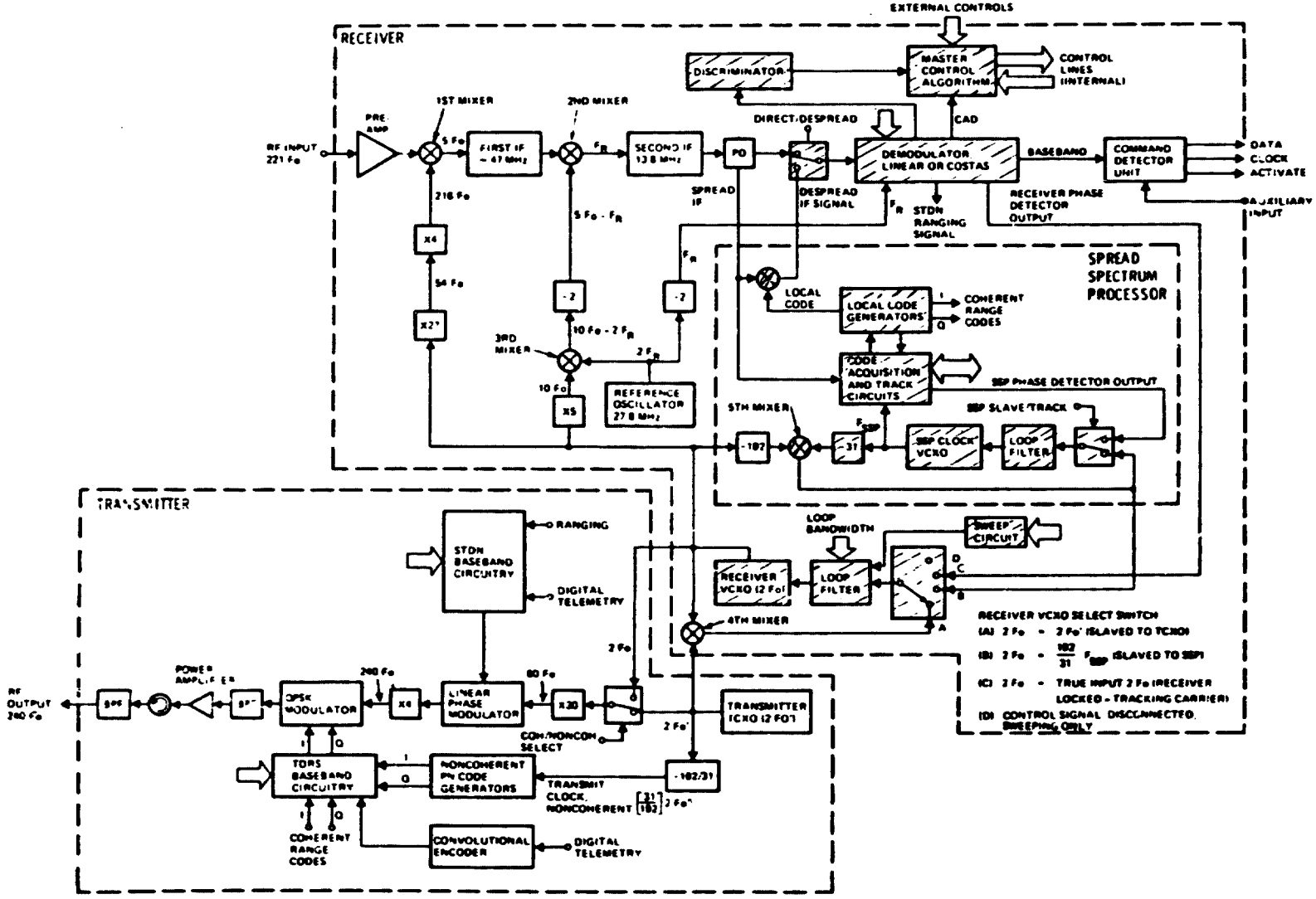

Figure 3. IUS STDN/TDRS Transponder Simplified Block Diagram with Shading of Functional Areas Analyzed and Reviewed

Since these same IUS memos are contained in the CDR data package, Axiomatix shall avoid duplication of effort by reviewing and critiquing only those memos which were not contained in the PDR package. In dealing with each of these analyses one by one, we shall simply refer to them by their IUS memo numbers, as per the entries in Table 1. It should also be pointed out that most of the analyses were performed by a single individual* (namely, Dr. Jack K. Holmes, Consultant to TRW) and thus it should not be surprising that comments made on one particular analysis might apply equally to many of the others. Such similarities in approach, style, etc., will be indicated in our discussion so as to avoid unnecessary redundancies.

*The remainder were performed by Dr. H. C. Osborne of TRW.

Table 1. IUS Memos Reviewed and Analyzed

Section	IUS Memo No.	Title
2. TDRS Mode--General	125	TDRSS Lock Detector Parameters, Structure and Performance for IUS
3. TDRS--Carrier Acquisition Analysis and Experiment	112	A Possible Problem in the IUS Code-Aided Carrier Acquisition Approach
	118	Improved Estimate of the Code-Multiplied Spectral Density
	114	Instantaneous Frequency Error of the Carrier Loop Reference (at the Moment of Code VCXO Disconnect)
	116	Instantaneous Frequency Error of the Carrier Loop Reference at the Moment of Code Loop Disconnect--Revisited
4. Costas Loop Performance--Analysis	115	Revision A--IUS Phase Detector Biases Due to Hybrid and Arm Filter Imperfections in the Costas Loop
	117	IUS Slip Time
	123	Influence of Arm Filter Delay on Tracking Performance of the IUS Costas Loop
5. SSP Analysis	110	Code Tracking Lock Detector Mean Time to Declare Out-of-Lock
6. STDN Dual Mode	122	STDN Dual Acquisition and Tracking Analysis
	124	Open-Loop Frequency Acquisition
7. STDN Only Mode	119	STDN Acquisition and Tracking Logic
	120	STDN Acquisition and Tracking Analysis
	121	IUS STDN-Only Discriminator Analysis for False Lock Avoidance

3.1.1 IUS Memo No. 125

This memo discusses the design and analyses of carrier lock detector performance for TDRSS dual-mode operation. In this mode, 2 kbps (125 bps in the low rate mode) data is modulated on the I-channel and modulo-two added to the command spreading PN (Gold) code while the ranging mode spread spectrum (truncated PN code) signal is modulated on the Q-channel. The power ratio of the I- and Q-channels is 10 dB.

The lock detector, in conjunction with the AGC amplifier, derives its error signal in the conventional manner from the I^2-Q^2 output of a Costas loop. This error signal, which has the identical SxS*, SxN and NxN components of the Costas loop tracking error signal, is filtered by a narrowband (with respect to the arm filter bandwidth) lowpass filter and the output is compared to a fixed threshold which is set at one-half the threshold (minimum C/N_0) signal level corresponding to the low data rate (125 bps) mode. The threshold outputs are used in a verification-type algorithm to decide whether or not the loop is in lock. In particular, two successive below-threshold indications must occur to assure that the lock detector declares the loop to be out of lock. If the loop is indeed in lock when this occurs, a false dismissal then occurs. One is interested in designing the mean false dismissal time to be quite long (perhaps on the order of years).

On the other hand, when the loop is out of lock and a given lowpass filter output sample exceeds the threshold, we have a false alarm. Here one is interested in keeping the probability of such an occurrence small so that the loop is not captured by frequent false alarms which then require the verification algorithm to produce two successive below-threshold indications in order to finally declare the loop truly out of lock.

In characterizing the performance of lock detection algorithms as described above, the theory of finite Markov chains is particularly useful. In this application, a three-state diagram is sufficient, with the transition probabilities determined from the lowpass filter output statistics. Since, as previously mentioned, the lowpass filter has a bandwidth which is narrow compared to that of the Costas loop arm filters,

---

*For this component, we must replace sin 2ϕ by cos 2ϕ.

the filter output may then be assumed to have Gaussian statistics, in which case, the transition probabilities take on the form of complementary error functions of a threshold-to-noise ratio. The effective amount of time one remains (dwells) in each state is determined by the time constant (correlation time) of the lowpass filter (for state 1) and the specified wait time after a below-threshold indication (for state 2).

Appendix I of this memo derives the mean and variance of the false dismissal time (the time to reach the absorbing state (#3) in the Markov chain). For a small probability of missed detection, the variance is shown to be approximately equal to the square of the mean, which is the same relation between the first two moments of an exponential distribution. Assuming such a distribution for false dismissal time, the author easily shows that the probability of falsely dismissing in t seconds or less is $1 - \exp(-t/\bar{T}_{FD})$, where $\bar{T}_{FD}$ is the mean false dismissal time.

Computations made from the above theoretical discussions reveal a mean-time-to-false-dismissal of greater than seven years (for either data rate) and a mean-time-to-dismiss a false alarm once the algorithm has been put in the tracking mode of 175 ms (for either data rate).

Based on the foregoing, the memo correctly concludes that false alarms will not "capture" the system (since their probability of occurrence is only 0.0016 and they are quickly dismissed) and false dismissals of true lock occur, on the average, infrequently enough (every seven years) so as to "never" cause a problem.

3.1.2 IUS Memos No. 112 and 118

The TDRS carrier acquisition analysis and experiment section of the CDR data package contains four* memos which can be arranged in two pairs, namely, 112 and 118, and 114 and 116. The second memo of each pair represents a revision of the first and, as such, contains the more meaningful results. Thus, we shall, in actuality, discuss only these second memos (118 and 116) while, at the same time, pointing out the changes made in the assumptions as given in the first memos (112 and 114).

IUS memo #112 calls attention to a possible problem (potential malfunction of the code loop and carrier lock detector during code loop loss of lock) in the IUS code-aided carrier acquisition approach. This

*Actually, there are five memos in this section, but one (#107) was included in the PDR and, as such, was previously critiqued.

approach consists of locking the receiver VCXO to a multiple (192/31) of the code loop VCXO with a CW loop, then multiplying this receiver VCXO output signal up to S-band (a factor of 110.5) to serve as the code loop input. The assumptions made in this memo are a 2-Hz single-sided code loop noise bandwidth at threshold ($C/N_0 = 34$ dB-Hz) and a carrier loop bandwidth much wider than the code loop bandwidth. As such, the interaction (cascading) of the carrier loop with the code loop was ignored and, thus, the carrier loop was assumed to do no more than scale the code loop phase noise process by the factor 192/31. Because of these oversimplifying assumptions, the results of memo #112 led to the conclusion that the code loop would potentially drop out in this mode and the carrier lock detector would not detect the presence of signal.

IUS memo #118 reconsidered the code-multiplied carrier acquisition problem under the assumptions of a 1-Hz (half as wide) code loop threshold bandwidth and an identical carrier loop threshold bandwidth. Certainly now the cascade of the code and carrier loop transfer functions further reduces the spreading of the code clock multiplied carrier produced by the multiplied-up phase noise of the code loop VCXO. Thus, despite the fact that the line component of the carrier power spectral density is essentially suppressed by the large phase noise obtained from the multiplied-up code clock, all the spread component (although much wider than the original phase noise process) is virtually contained within a ±100 Hz bandwidth. In conclusion, then, the very wideband estimates of the code-multiplied carrier power spectral density made in IUS memo #112 which could potentially cause the code loop to drop out in this mode were, in IUS memo #118, refined to the point where it may be safely concluded that the IUS code-aided carrier acquisition technique is viable.

Axiomatix has carefully reviewed the analyses performed in these two memos and agrees with the conclusions drawn therein.

3.1.3 IUS Memos No. 114 and 116

This second pair of memos in the TDRS carrier acquisition analysis and experiment section addresses the problem of predicting the instantaneous frequency error in the carrier loop just after disconnecting the code loop VCXO when, prior to that time, the carrier loop was configured to track a scaled version of the code loop clock. Indeed, an accurate

estimate of this instantaneous frequency error is essential in deciding whether or not the carrier loop bandwidth is sufficient to pull in this frequency offset during acquisition.

Clearly, when the carrier loop is connected to the code loop VCXO, an instantaneous frequency error Δf in the code loop would produce a carrier frequency offset equal to $(192/31)x(110.5)\Delta f = 684.4\ \Delta f$. Here the first factor represents the scaling of the PN code clock at the receiver VCXO input, and the second factor is the multiplication required to bring this reference up to S-band. Thus, a one-sigma code loop frequency error at threshold ($C/N_0 = 33$ dB-Hz) on the order of 13 Hz (see IUS memo #117) would produce, before disconnect, a carrier frequency offset of $(684.4)(13) = 8897.2$ Hz, which is so large that the carrier loop could never acquire with any reliability. When the code loop VCXO is disconnected, however, the action of the code loop and carrier loop filters reduce this frequency offset considerably, in particular, to a value well within the frequency acquisition range of the carrier loop.

In IUS memo #114, the assumption is again (as in IUS memo #112) that the carrier loop is wide compared to the code loop. Thus, the approach taken in memo #112 was to compute (approximately) the standard deviation of the voltage on the capacitor in the code loop filter, then simply scale this quantity by the factor $(192/31)(110.5) = 684.4$ to arrive at the carrier (one-sigma) frequency offset at S-band*. Multiplication of this result by three (to give a three-sigma value) was then used to give a rough estimate of the required carrier loop bandwidth during acquisition.

Interestingly enough, the computed value of carrier frequency offset, namely, $(192/31)(110.5/4)x(0.155\ \text{Hz}) = 26.5$ Hz (0.155 Hz was the computed one-sigma value of code loop filter capacitor voltage) was in excellent agreement with a measured value in the laboratory of 25 Hz. Unfortunately, however, this was just a coincidence apparently caused by nullifying errors in the assumptions made in the analysis. In particular, the variance of the capacitor voltage as given by equation (115) of this memo is in $(\text{rad/sec})^2$, not $(\text{Hz})^2$, since the code loop VCXO gain, K_v, is

*Actually, the laboratory measurements were made at 25% of the final S-band frequency; thus, the appropriate multiplication factor for comparison of theory and experiment is $(192/31)(110.5/4) = 171.1$.

in rad/sec/V. Thus, the calculated value of carrier frequency offset given previously, namely, 26.5 Hz, should be divided by 2π, which results in 4.2 Hz. Furthermore, as discussed in IUS memo #116, the wideband carrier loop assumption must be revoked in favor of a loop whose bandwidth is identical to that of the PN code loop. When the two loops are now considered in cascade, the problem must be reformulated to directly compute the RMS voltage (due to frequency offset) on the capacitor in the carrier loop filter. When this is done (as in memo #116), along with the 2π-factor correction previously discussed, then the one-sigma (RMS) frequency error at S-band becomes (192/31)(110.5)x(0.01 Hz) = 6.84 Hz or, at the laboratory measurement frequency, (192/31)(110.5/4)x(0.01 Hz) = 1.71 Hz. These numbers correspond to threshold loop conditions, namely, both loop dampings are at 0.707 and both loops have a bandwidth of 1 Hz.

Now since the theoretical values of frequency offset error are considerably less than laboratory measurement values, the author points out that this may be true because the analysis ignores the effects of logic noise and oscillator noises. Indeed, since a large discrepancy exists between measured and theoretical values, one might suggest that these other unaccounted for effects tend to dominate. We hasten to add, however, that estimates of oscillator noise and, in particular, logic noise are difficult to come by, which makes accounting for these effects analytically all the more difficult.

3.1.4 IUS Memo No. 115

This is the first memo in the Costas loop performance analysis section of the CDR to be critiqued and discusses the static tracking phase error induced by thermal noise biases at the output of the loop's third multiplier. The two sources of bias discussed are an imperfect (other than 90°) input hybrid and a combination of arm filter mismatch and input bandpass filter asymmetry. Their effects in producing static phase errors are treated independently.

In the hybrid misalignment analysis, the hybrid is modeled as producing a pair of "quadrature" demodulation reference signals which are separated in phase by $90° + \delta\theta$, the quantity $\delta\theta$ representing the hybrid angle error. When computing the phase detector outputs due to signal only

(as in eq. (10)), the author commits an error in that he ignores the hybrid angle error. Thus, his final result for static phase error (eq. (14)) includes only the effect of hybrid angle error on the noise component at the third multiplier output, which indeed turns out to be the less dominant effect. To correct this error, we suggest that equations (10), (11), (12) and (14) read as follows:

$$e_c(t) = \sqrt{P}\,\tilde{d}(t)\cos\phi \;;\; e_s(t) = \sqrt{P}\,\tilde{d}(t)\sin(\phi-\delta\theta)\;, \qquad (10)$$

$$\begin{aligned}\bar{e} &= \alpha P \sin(\phi-\delta\theta)\cos\phi \\ &= \alpha P\left[\frac{\sin(2\phi-\delta\theta)}{2} - \frac{\sin(\delta\theta)}{2}\right]\;,\end{aligned} \qquad (11)$$

$$\left(\frac{\overline{\tilde{n}_c^{\,2}}}{\alpha P} + 1\right)\delta\theta = \phi_{ss}\;, \qquad (12)$$

and

$$\boxed{\phi_{ss} = \left(\frac{N_0\pi f_0}{2\alpha P} + 1\right)\delta\theta}\;. \qquad (14)$$

Then, for the case where $R_b = 2000$ bps, $f_0 = 2000$ Hz, $\alpha = 0.84$, and $P/N_0 = 43$ dB-Hz (includes 1-dB despreader loss), Table I of the memo, which tabulates static phase error versus hybrid angle error, should be modified as follows:

$\delta\theta(^\circ)$	$\phi_{ss}(^\circ)$
1	1.187
2	2.375
3	3.56
4	4.75
5	5.94

Thus, the statement made in the summary of the memo, namely, that "the steady-state error is about 1/5 of the hybrid angle error" should be changed to read "the steady-state error is slightly greater than the hybrid angle error."

The second part of this memo assumes a perfect (90°) input hybrid and examines the effects of mismatched arm filters and an input bandpass filter (BPF) with an asymmetric frequency response around its center frequency. In particular, the two lowpass arm filters are assumed to be one-pole RC filters with different 3-dB cutoff frequencies, namely, f_1 and f_2, and the asymmetry in the equivalent lowpass version of the input BPF is modeled as a linear "tilt" in the corresponding power spectral density, namely,

$$S_L(f) = \frac{N_0}{2}(1 + af); \quad |f| \leq 5 \text{ kHz}.$$

The author then shows that the static phase error produced by these two sources of filter imperfection is given by

$$\phi_{ss} = \frac{\pi}{4}\left(\frac{aN_0}{\alpha P}\right)(f_2 - f_1)f' \quad ,$$

where many simplifications in the analysis were made by letting f' equal f_1 or f_2 in some of the manipulations.

For a 0.1 dB tilt at f = 5 kHz, ($10 \log_{10}(1 + ax5x10^3) = 0.1$, or $a = 4.88x10^{-6}$), $\alpha = -0.5$ dB, $P/N_0 = 43$ dB-Hz, $f_1 = 1948.3$ Hz and $f_2 = 2096.6$ Hz, the computed value of ϕ_{ss} (assuming $f' = f_2$) is 0.0038°. The memo follows with a table which computes ϕ_{ss} for larger values of tilts. The latter three values of ϕ_{ss} in this table, corresponding to respective tilts of 0.3, 0.5 and 1.0 dB, should be corrected to read 0.0108, 0.018 and 0.0392°.

One further point of correction, although probably of second-order importance, deserves mention at this time. The parameter α in the above equation which ordinarily characterizes the arm filtering degradation on the SxS term in the loop when both arm filters are identical should be modified for the case where the arm filters are different. In particular, we would now have (analogous to eq. (42)) for the noise effects

$$\alpha = \frac{1}{2}\int_{-\infty}^{\infty}\left[H_1(\omega)\,H_2^*(\omega) + H_1^*(\omega)\,H_2(\omega)\right] S_d(\omega)\,\frac{d\omega}{2\pi}$$

where $S_d(\omega)$ is the data modulation spectrum and $H_1(\omega)$, $H_2(\omega)$ are the arm filter transfer functions, i.e.,

$$H_i(\omega) = \frac{1}{1 + j\frac{f}{f_i}} \quad ; \quad i=1,2$$

Substitution of $H_i(\omega)$ into the above expression for α and simplifying yields

$$\alpha = \int_{-\infty}^{\infty} \frac{\left(1 + \frac{\omega}{\omega_1}\right)\left(1 + \frac{\omega}{\omega_2}\right)}{\left(1 + \left(\frac{\omega}{\omega_1}\right)^2\right)\left(1 + \left(\frac{\omega}{\omega_2}\right)^2\right)} S_d(\omega) \frac{d\omega}{2\pi}$$

which, for a small 3-dB cutoff frequency difference, is approximately α, as previously computed for identical arm filters.

Thus, in conclusion, the hybrid imperfection effect dominates over the imperfect filtering effects, and the static phase error induced is on the order of the hybrid angle error.

3.1.5 IUS Memo No. 117

The mean slip time of the carrier-tracking loop in the IUS-TDRS transponder is computed at both threshold conditions (C/N_0 = 33.7 dB-Hz, R_B = 125 bps) and strong signal conditions (C/N_0 = 43.7 dB-Hz, R_B = 2000 bps). The loop is configured as a standard Costas loop with an input signal having an unbalanced QPSK format characterized as follows. The received signal has a PN spread data modulation on the strong (I) channel and PN only on the weak (Q) channel. The power ratio is fixed at 10:1. After being despread by the I-channel PN code, the signal retains an unbalanced QPSK format with data modulation only (assuming "perfect" despreading with a fixed despreading loss) on the I-channel, and PN only (the product of the in-phase and quadrature PN codes) on the Q-channel. This signal serves as the Costas loop input. As such, the evaluation of the loop's phase error variance due to thermal noise follows along the lines of previous analyses of biphase Costas loops with passive arm filters and unbalanced QPSK inputs. In making this statement, we tacitly make the assumption that the

PN code on the Q-channel behaves as a random data modulation of rate $R_c = f_c$, where f_c is the PN chip rate (i.e., 3×10^6 Mchips/s). Thus, it is not surprising that eq. (22) of the memo agrees with [1, eqs. (28) and (30)] after the appropriate changes in notation.

Next, the memo evaluates the phase error variance component due to oscillator phase noise. The phase noise model, based on IUS phase noise specifications, was assumed to have a power spectral density which varied as K/f^6. For simplicity of computation of the phase error variance due to phase noise, the out-of-band loop transfer function $1 - H(f)$ was assumed to behave like a "brick wall" filter having zero value below the loop natural frequency and unity value above this frequency. Finally, the two phase error variance components (that due to thermal noise and that due to oscillator phase noise) are added to give the total phase error variance $\sigma_{2\phi}^2$.

Before determining the mean slip time of the Costas loop, one needs, in addition to the total phase error variance, the steady-state phase error due to dynamics such as a residual carrier frequency rate of Δf Hz/sec. For a second-order Costas loop, these two parameters are related by

$$2\phi_{ss} = 2\left(\frac{2\pi\Delta\dot{f}}{\omega_n^2}\right) \tag{1}$$

where ω_n is the loop's radian natural frequency which, for a 0.707 loop damping, is related to the loop bandwidth B_L by $\omega_n = 1.89\ B_L$. Having now determined $\sigma_{2\phi}^2$ and ϕ_{ss}, the author computes mean slip time $\overline{T}$ (normalized by the loop bandwidth) from the formula

$$B_L\overline{T} = 1.5 \exp\left[\frac{1.2}{\sigma_{2\phi}^2}\left(1 - \sin 2\phi_{ss}\right)\right]$$

$$= 1.5 \exp\left\{\frac{1.2}{\sigma_{2\phi}^2}\left[1 - \sin\left(\frac{4\pi\Delta\dot{f}}{(1.89)^2 B_L^2}\right)\right]\right\} \tag{2}$$

This relation is valid for a second-order Costas loop with an active loop filter and was originally obtained from simulation results on an analogous phase-locked loop.

The author concludes with an evaluation of (2) for threshold and strong signal conditions, and $\Delta\dot{f}$ = 70 Hz/sec. At threshold, a value of B_L = 25 Hz maximizes $\bar{T}$, whose value is 6000 sec (10 min). In the absence of phase noise and loop dynamics ($\Delta\dot{f}$), $\bar{T}$ is monotonically decreasing with increasing B_L. At strong signals, the same B_L = 25 Hz produces $\bar{T} \gg 10^4$ min.

The results given in this memo are obtained by straightforward application of previously derived results and, as such, need no further investigation.

3.1.6 IUS Memo No. 123

The effect of the delay induced by the arm filters in the IUS-TDRS Costas loop on loop bandwidth and, hence, the phase error variance, is investigated. The key step in the analysis is the approximation made with respect to the signal $e_u(t)$ appearing at the upper arm filter output, namely, that the effect of this filter on the data modulation and the loop phase error are separable. More specifically, letting H(s) denote the arm filter transfer function, then

$$e_u(t) = \sqrt{P}\, H(p)[d(t) \sin \phi(t)] \qquad (1)$$

which, for small ϕ. becomes

$$e_u(t) \cong \sqrt{P}\, H(p)[d(t)\, \phi(t)] \qquad (2)$$

is approximated by

$$e_u(t) \cong \sqrt{P}\, (H(p)\, d(t))(H(p)\, \phi(t)) \qquad (3)$$

where p has been used to denote the Heaviside operator. It is argued that (3) follows from (2), provided that "the lowpass arm filter H(s) does not seriously distort the baseband data stream." Although there appears to be no approximate mathematics that can lead one from (2) to (3), there is a

reasonable plausibility argument that one can use to make this step somewhat believable. Typically, the $\phi(t)$ process being slowly varying with respect to d(t) appears as an envelope modulation on d(t) which, when passed through the arm filter, is essentially unaffected in amplitude but is shifted (delayed) by the arm filter group delay Thus, if we approximate $\phi(t)$ as a single-frequency (say, ω_0) beat note, then $H(t)\ \phi(t) \tilde{=} \phi(t - t_0)$, where $t_0 = \arg H(j\omega_0)/\omega_0$ is a good approximation to the envelope modulation on the filtered data stream.

Making the above approximation, the author proceeds to find a simple relation between the loop bandwidth (including the arm filter delay effect), say $B_L(D)$, and the zero-delay loop bandwidth B_{LO}, namely,

$$\frac{B_L(D)}{B_{LO}} = \frac{1}{1 - \frac{D}{2\zeta}} = \frac{\sigma_\phi^2(D)}{\sigma_{\phi 0}^2} \tag{4}$$

where ζ is the loop damping and $D = \omega_{no}\tau$, with ω_{n0} the zero-delay radian natural frequency and τ the time constant of the single-pole arm filter H(s). Since ω_{n0} and B_{LO} are related by

$$\omega_{n0} = 2B_{LO}\left(\frac{4\zeta}{1 + 4\zeta^2}\right) \tag{5}$$

then (4) can be alternately be written as

$$\frac{B_L(D)}{B_{LO}} = \frac{1}{1 - \frac{4B_{LO}\tau}{1+4\zeta^2}} = \frac{\sigma_\phi^2(D)}{\sigma_{\phi 0}^2} \tag{6}$$

Clearly, the mean-square phase jitter with delay becomes unbounded when

$$B_{LO}\tau = (1 + 4\zeta^2)/4\ . \tag{7}$$

For $\zeta = 0.707$, $B_{LO} = 75$ Hz and a 100-Hz 3-dB cutoff frequency (i.e., $\tau = 1/2\tau(100) = 0.00159$), the increase in RMS phase jitter is only 9% ($\sigma_\phi(0)/\sigma_{\phi 0} = 1.09$).

The author follows the computation of mean-square phase jitter with a discussion of the effect of the arm filter delay on loop stability, as determined by Routh's stability criterion, and the root locus plot. The interesting (but not too surprising) result is that the loop bandwidth at which the loop becomes unstable is also determined from (7), namely, the same value at which the mean-square phase error variance becomes unbounded.

Finally, we wish to call attention to a similar study [2] with similar results in which the effect of delay on the loop bandwidth and stability of a data-aided loop (DAL) were investigated, thus lending more credibility to the analysis performed in this memo. The DAL, which is also used for tracking suppressed carrier signals, has much similarity to the conventional Costas loop.

3.1.7 IUS Memo No. 110

This memo is the only one in the SSP analysis section which was not previously critiqued by Axiomatix. In particular, it addresses the mean time to declare out-of-lock for the code-tracking loop, both when the signal is present and when it is absent. The lock detector algorithm is of the "n-out-of-n" type wherein n (typically, 16) successive below-threshold events are required to declare an out-of-lock condition. If an above threshold even occurs anywhere along the way, the algorithm returns the system to its initial state and resets the below-threshold count to zero.

The mean time to out-of-lock performance of such a discrete time lock detector algorithm is best determined by modeling the algorithm as a 17-state Markov chain (the 17th state being the absorbing state, namely, an out-of-lock declaration) and applying the well-known theory for such chains to this particular case. Actually, for $n \leq 5$, a formula for this mean-time performance was determined by brute force (direct) calculation in a previous memo by the author (see TRW IOC No. SCTE-50-76-275/JKH). Thus, this memo serves to merely formalize the

validity of this result for all values of n. In particular, the mean time to out-of-lock, $\bar{T}$, is simply given by

$$\bar{T} = \frac{q^{-n}-1}{1-q} T_{DWELL}$$

where T_{DWELL} is the dwell time per state (assumed equal for all states), i.e., the time between threshold tests of the integrator output, and q is the probability of a below-threshold event for any given threshold test.

Since, when signal is absent, q = 0.95 and, when signal is present, q = 0.5, then for n = 16 and a 50-ms dwell time, the corresponding values of T are found to be 1.27 seconds and 109.2 minutes, respectively.

The straightforward nature of these results and the absence of complicating assumptions requires that no further investigation be performed.

In the STDN dual mode section of the CDR package, two memos were written which pertain to the analysis and design of the lock detector, noncoherent, AGC and open-loop frequency acquisition circuits associated with the carrier-tracking loop of the IUS transponder. Since the first of these two memos (#122) assumes knowledge of the second (#124), we shall start by critiquing the second.

3.1.8 IUS Memo No. 124

In the STDN dual mode of the IUS transponder, an open-loop frequency acquisition scheme is used which involves linear sweeping of the VCO frequency to bring the initial frequency uncertainty within the pull-in range of the loop (typically on the order of the loop bandwidth). Since the loop is open during this sweep interval, an auxiliary detection circuit must be used to determine when to remove the sweep and simultaneously* close the loop. This auxiliary detector consists of a coherent amplitude detector (CAD) followed by a lowpass filter and threshold device.

---

*In the actual frequency acquisition scheme used in the STDN mode, the sweep continues for an additional 4 ms after the detector indicates acquisition has been achieved to all for the processing time of the microprocessor which controls the closing of the loop.

An instantaneous crossing* of the threshold by a signal at the input to this device indicates acquisition whereupon the sweep is terminated and the loop closed.

Such a half-wave rectifier type of open-loop frequency search circuit has been previously described in [3]. This memo discusses its application to the IUS transponder in the STDN dual mode. In particular, computer simulation and laboratory test results are obtained for the waveforms at the output of the lowpass RC decision filter (in the absence of noise) so as to enable selection of this filter's 3-dB cutoff frequency β for a given sweep rate R (Hz/sec), normalized (to the peak signal amplitude) threshold level δ, and closed-loop bandwidth f_1. Indeed, it is shown that if, for a given initial frequency offset outside the loop's pull-in range, β is too small, then, depending on the initial phase difference ϕ_0 between the input signal and the swept VCO, the threshold may or may not be exceeded as the VCO is swept through the pull-in range. Increasing β helps this situation; however, if β is too large, then the threshold is exceeded while the loop is still outside its pull-in range. Hence, the sweep will be terminated and, consequently, the loop closed prematurely.

The author provides what appears to be a reasonable rule of thumb for the selection of β, namely, the peak value of the normalized detector output frequency response H(f), evaluated at the edge of the pull-in range (assumed equal to the loop bandwidth f_1) should be less than the normalized threshold δ. For a single-pole decision filter (β = 3-dB frequency), it is straightforward to show that the above is equivalent to the condition†

$$\beta < \frac{f_1 \delta}{\sqrt{1-\delta^2}}$$

---

*Again, because of the 4-ms processing time of the microprocessor, a "stretching" or hold circuit follows the threshold detector to prevent situations where the input signal reverses and falls below threshold in less than 4 ms, i.e., sharp peaks.

†The author does not actually write this inequality in this form although it is obtained by obvious steps from the results given therein. Also note that this result is independent of the sweep rate R although the actual simulation results were performed for $R=40\times10^3$ Hz/s.

Thus, for $\delta = 0.5$ and $f_1 = 400$ Hz (STDN parameters), we obtain $\beta < 400/\sqrt{3} = 231$ Hz (the author uses the approximate value 250 Hz).

The next area of investigation was the calculation of acquisition probabilities which were performed by computer simulation (in the absence of noise) in view of the difficulty of obtaining these results analytically. Note again that, although the additive noise was assumed to be absent, the probability of acquisition is, in general, less than one due to dependence of the acquisition process on the initial phase difference ϕ_0. The author compares the acquisition probability results obtained by the above-mentioned simulation with experimental results obtained in [3]. In some cases, there appears to be reasonable agreement whereas, in other cases, there seems to be no match at all. Since, for the latter situation, the author of [3] does not state to which of the three possible open-loop implementations (one mixer and one half-wave rectifier, one mixer and one full-wave rectifier, or two mixers and two full-wave rectifiers) his results apply, one is unable to resolve the discrepancy. Herein lies one of the principal reasons for issuing IUS Memo #124 in the first place, namely, to point out the lack of agreement between the previously published experimental results and the computer simulation results obtained by the author of the memo.

Finally, this memo concludes with a discussion of how the results might be extended to account (in a very rough sense) for the effects of additive noise.

In the opinion of Axiomatix, the results documented in this memo represent a significant contribution to the understanding of the performance and behavior of open-loop frequency acquisition techniques of the type described therein. As such, the results are given in a sufficiently general parametric form as to be useful in applications outside of the IUS transponder. Perhaps the only area which would require further investigation would be the noise-present case, where computer simulation could again be used (although with more difficulty) rather than the rough extension (valid only for high SNR) approach given in the memo. Indeed, the entire subject of frequency acquisition in noise is an area of research where much needs to be done.

3.1.9 IUS Memo No. 122

Associated with the open-loop frequency acquisition technique described in IUS Memo #124 is the lock detector of the STDN dual mode whose functions are to close the tracking loop and stop and sweep* when frequency acquisition has been completed. The indication that frequency acquisition is complete is a high (above threshold) signal from the sampled-and-held output of the threshold device in the frequency acquisition circuit. Thus, this signal serves as the input to the lock detector whose control algorithm is as follows: When the loop is initially open, a single high sampled-threshold output shall close the loop. Two successive high-threshold outputs are required to terminate the sweep. Also, when the loop is initially closed and in lock, two successive low-threshold outputs are required to open the loop and reinstate the sweep.

The purpose of this memo is to determine decision filter bandwidth and threshold settings for the above circuit, taking into account both the hold circuit at the sampled-threshold output and the noncoherent AGC (NAGC) which accompanies the loop. As in the previous lock detector analyses (see IUS Memos #125 and 110), the theory of finite Markov chains is used to determine the mean time to false alarm (falsely close the loop and falsely disable the sweep) performance. Other computations include probability of false alarm (falsely closing the loop and falsely disabling the sweep) and accidental restart (falsely open the loop).

For the NAGC effects, the author assesses the increase in AGC gain in going from acquisition (S/N_0 = 46 dB-Hz) to tracking (effective† S/N_0 = 40 dB-Hz) as a function of the AGC filter bandwidth. Also determined is the further increase in gain (up to a practical limit) when only noise is present. The analyses performed here is similar to that done in IUS Memo #125 and, as such, requires no further explanation. Similarly, the false alarm and accidental restart probability calculations parallel those performed in IUS Memo #125 (except for the effect of holding the threshold output sample for 4 ms, which is shown to roughly double the false alarm probabilities which would be calculated for an instantaneous

---

*Actually, the lock detector telemeters a message to the ground and the ground stops the sweep.

†The actual S/N_0 during tracking is 43 dB-Hz; however, the additional suppression caused by the presence of command modulation and, possibly, two ranging tones, both phase-modulated on the carrier, is 3 dB.

sampling operation). Since the loop is closed after the first threshold crossing and the sweep disabled after the second threshold crossing, the author computes the "instantaneous" probability of falsely disabling the sweep as the square of the probability of falsely closing the loop. This is only approximately correct since the probability of exceeding the threshold the second time must be computed with the loop closed, while the probability of exceeding the threshold the first time is computed with the loop open. In general, these two threshold crossing probabilities will be different, depending on how far out of lock (amount of frequency offset relative to the loop's pull-in range) the loop is by the time of the second threshold crossing.

Analogous to the difference in the false alarm probabilities for closing the loop and disabling the sweep, the mean time to occurrence of these false alarm events must be computed from different Markov state models. For the former, the mean time is simply

$$\overline{T}_{close} = \frac{T_0}{p}$$

where T_0 is the threshold sampling time interval (i.e., 4 ms) and p is the threshold crossing probability when the loop is out of lock. For the latter, the mean time is*

$$\overline{T}_{disable} = \frac{T_0 + (1-q)\,T_1}{(1-q)^2}$$

where T_1 is the time the loop remains closed after the initial closure before the threshold is again sampled, and $1-q$ is the probability of exceeding the threshold when the loop is in lock. Here again, the above result is only approximately correct since it assumes that the transition probabilities from state 1 (loop closed) to state 2 (sweep disabled) are the same as those from state 0 (loop open) to state 1.

*The author's result for this quantity, namely,

$$T_{disable} = \frac{T_0\,(1-q)\,T_1}{(1-q)T_1^2}$$

is incorrect although the numerical evaluation appears to be correct.

To compute the probability of accidental reopening of the loop, the author points out that three cases can occur. For the first case, the assumption is that the loop has locked but the sweep is still on; hence, the loop is tracking the sweep with a steady-state phase error equal to the arc sine of the ratio of the sweep rate to the square of the loop's natural frequency. For the second case, the loop is tracking, but the NAGC has not yet had time to act. Finally, the third case is the same as the second except that the NAGC has now had time to act. This last case yields the largest restart (reopening of the loop) probability and, hence, represents the worst case.

The memo concludes with the corresponding mean-time-to-loss-of-lock calculations which employ a Markov state model analogous to that used in computing mean time to disable the sweep, the difference being that the above-threshold probabilities are switched with below-threshold probabilities and the latter computed assuming an in-lock condition, i.e., tracking.

In summary, the computations are straightforward applications of the Markov chain approach, the theory of which was documented in previous IUS memos. Thus, other than the modifications to include such effects as sample-and-hold time, the results are analogous to those previously obtained for the TDRS carrier and PN code loops.

3.1.10 IUS Memos No. 119 and 120

These two memos are for the STDN-only mode, the companions to IUS memos 124 and 122 for the STDN dual mode of operation. Again, the purpose of the documentation is to characterize the behavior and analyze the performance of the acquisition and lock detector schemes, along with a determination of the necessary threshold settings. Although, in principle, three possible frequency acquisition schemes are under consideration, namely, (1) an open-loop scheme similar to that for the STDN dual mode, (2) an existing digital hardware version of a closed-loop scheme and (3) a software implementation of (2), only the second scheme (also referred to as the DOD version) is discussed in these memos. Since this scheme is referred to as a "closed" loop frequency acquisition technique, it implies that the VCO is swept with the loop closed and, thus, a high

(greater than threshold) signal out of the lock detector is used only to stop the sweep. In reality, the VCO is initially swept open-loop and can be immediately (with no delay) closed by a low (less than threshold) output from an auxiliary discriminator circuit prior to a lock detector threshold crossing, or subsequently (after a short delay) by a lock detector (high) signal* itself, with the former being the more likely to occur. Once the loop is closed, however, only the lock detector output signal both stops the sweep and maintains the closed loop after the sweep has stopped. It is in this sense that the behavior of the lock detector is analogous to that of the STDN dual mode of operation.

The behavior of the actual closed-loop frequency-searching circuit employed closely parallels that previously described in [3], the main difference being that, during the initial part of the sweep, the loop is open until closed by the discriminator. In addition, after the loop is closed and the sweep has been stopped, the loop bandwidth is narrowed for the tracking mode of operation.

Assuming that the loop has locked and reached the steady state (the discriminator has previously indicated that the loop be closed), but the sweep has not yet been removed. The DC output of the coherent amplitude detector (CAD) is then simply given by

$$u_0 = \sqrt{S_1}\, J_0(1.1)\sqrt{1 - \left(R/\omega_n^2\right)^2} \qquad (1)$$

where S_1 is the signal power at this point, $R/2\pi = 10^6$ Hz/sec is the sweep rate, and $\omega_n = 1.89\ B_L = 3780$ rad/sec is the natural frequency of the loop, with $B_L = 2000$ Hz the loop noise bandwidth. The $J_0(1.1)$ factor occurs because the input carrier is phase modulated by a data-modulated 16 kHz sinusoidal subcarrier with modulation index 1.1 radians. Thus, once S_1 is determined (depending on the action of the noncoherent AGC), u_0 is specified. Furthermore, the variance of the noise at the CAD filter output also depends on the NAGC action, i.e., whether or not signal is

*Actually, two possibilities exist here, namely, a single high pulse of greater than 3-ms duration, or two or more short (less than 3-ms duration) pulses within 33 ms (but greater than 3 ms apart) will close the loop after a total delay of 36 ms after the leading edge of the first pulse.

present. The AGC gain is normalized such that it has value unity when signal is present and $S/N_0 = 52$ dB-Hz. Thus, when signal is present, the CAD decision filter output has a DC value given by (1) with $S_1 = S$ and a noise variance $\sigma_{u_1}^2 = N_0 B$, where B is the noise bandwidth of this filter (a single-pole RC filter). When signal is absent, the DC output is zero and the noise variance is

$$\sigma_1^2 = \left(1 + \frac{S}{N_0 B_{AGC}}\right) N_0 B \qquad (2)$$

where B_{AGC} is the noise bandwidth of the AGC input filter [also, a single-pole RC with 3-dB cutoff frequency of 1600 Hz, i.e., $B_{AGC} = (\pi/2)(1600)$]. Using these relations and some additional results given in [3] for probability of successful acquisition, it is a relatively straightforward matter to compute the false alarm and detection probabilities associated with the action of the lock detector in stopping the sweep. One further assumption is made that the threshold δ is chosen equal to half the DC value of the decision filter output corresponding to signal present, i.e., $\delta = 1/2\ u_0$, where u_0 is given by (1). This yields (for a decision filter bandwidth of 200 Hz) a false-alarm probability* of 10^{-3}.

3.1.11 IUS Memo No. 121

(a) Introduction

The purpose of this memo is to give an approximate analysis of a discriminator used to avoid false locks and to specify the filter bandwidths and number of poles needed for these filters. The two latter tasks seem to be rather straightforward, and no major objections arise, at least insofar as the resulting SNR is the dominant measure of performance for the last case.

The analysis of the discriminator is basically composed of two similar parts: Case A/B and Case C. The first part (A/B) tries to estimate the probability that, as it sweeps through the subcarrier component

*Actually, this false alarm probability is the probability that two or more samples of the CAD decision filter output exceed the threshold δ in a 65-ms interval.

of the spectrum (as shown in Figure 4), the discriminator will indicate a voltage below threshold which would imply a false-lock case. In other words, the phase-lock loop would track that component, while the discriminator would falsely indicate (by being below threshold) that this is actually the carrier component. Ideally, this would not occur if noise were not present because the discriminator window centered at the first subcarrier harmonic would "see" an asymmetric spectrum, consisting mainly of the carrier component at the edge, and would thus produce an output above the threshold. Note that the distance between the carrier and the first subcarrier is 16 kHz, while the discriminator window is 25-kHz wide (one-sided). Hence, the carrier is well within its reach when the window's center is at $f_{carrier} + f_{subcarrier}$. Therefore, it is the noise which might cause a false indication. Hence, the analysis of section C has a similar objective and it addresses the case where the discriminator is centered at the carrier which should, ideally, provide an indication below threshold. The analysis then aims at the probability of false rejection. Since the analytical tools are identical in both cases, we examine in detail only the first. It should be stated that the overall system is highly complicated (nonlinear/time-varying/stochastic), and thus, it is possible that both the original analysis and our critique can be subjected to further questions regarding the accuracy of some of the approximations and analytical techniques. In all fairness, however, we should recognize that the analysis is very close to the limits of analytical techniques, exempting, of course, any numerical mistakes and, possibly, some minor theoretical improvements. We note at the very onset of the analysis however, that there is a fundamental question concerning the validity of the approach. The question is: since the system is time varying (because of the sweeping process), can steady-state analysis provide credible results, especially when calculating noise variances? Assuming that the above is answered positively (otherwise, the whole analysis collapses), we will proceed with side observations/corrections/improvements, as listed below, further indicating which ones might bear significance to the final results.

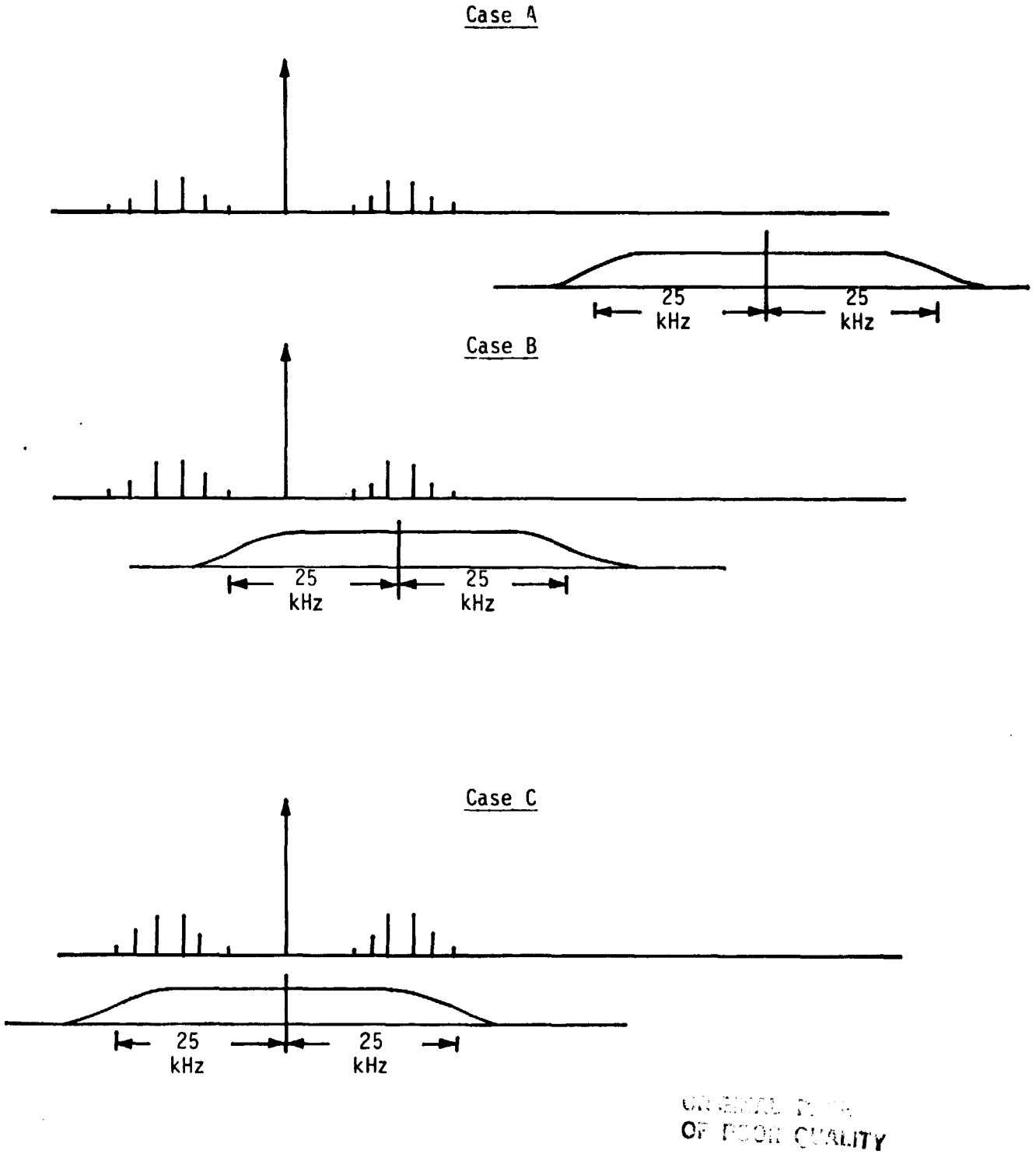

Figure 4. The Three Cases of Discriminator Detection of Interest

(b) Specific Comments

Since the carrier-tracking loop is a phase-lock loop, it should not lock to the subcarrier if the subcarrier is biphase modulated by completely random data. This modulation, of course, results in a $(\sin x/x)^2$ spectrum. If there is a periodic component or long string of all zeros or all ones, however, in this data, then the carrier loop can lock. Thus, the analysis performed by the author is a worst-case analysis since it assumes no data modulation on the subcarrier.

The author's expression for sweep rate as determined by Viterbi (7) has an extra factor of 10^6 in it and should be stated as

$$R_{NF} = \frac{1}{2}\pi\frac{\omega_1^2}{2} = 1.14 \text{ MHz/sec.}$$

Likewise, the sweep/rate for the STDN-only mode (8) has an extra factor of 10^6 and should be stated as

$$R = 1 \text{ MHz/sec.}$$

Also, the expression for the outputs of the in-phase and quadrature multiplexers, (19) and (20), erroneously have ω_1 rather than ω_0, and the expressions for the arm filter outputs of these signals, $\tilde{e}_c(t)$ and $\tilde{e}_s(t)$ ((24) and (28)), should have $\tilde{n}_1(t)$ and $\tilde{n}_2(t)$ for the noise terms rather than $n_1(t)$ and $n_2(t)$. We also note that, by introducing a $\Delta\omega$ parameter ($\Delta\omega$ = frequency from $f_{carrier} + f_{subcarrier}$) and proceeding with the analysis, one assumes that $\Delta\omega$ is fixed, a contradiction to the very fact of the sweeping mechanism. Pursuing this, we see that the factor $H_1^2(\Delta\omega)$ has been omitted from the expression for the input SNR, ρ_i, for the limiter (48). Correctly stated, ρ_i is given by

$$\rho_i = \frac{P\, J_1^2(1.1)\, H_1^2(\Delta\omega)}{2\, N_0 B_1}$$

The significance of that is rather minor if $\Delta\omega$ is assumed to be well within the flat portion of the filter. However, $\Delta\omega$ is variable with time. Furthermore, in the expression for ρ_i, the author has used $J_1^2(1.1)$ incorrectly, instead of $J_0^2(1.1)$. This means that the numerical evaluation of ρ_i should be corrected accordingly. Thus, ρ_i should be -3.48 dB

(not 0.24 dB), or a factor of 0.4468 (not 1.06). Since the SNR ρ_i is used to evaluate the noise variance, the error might be important in the sense that the noise is underestimated.

The noise spectra calculated by the author and shown in Figure 5 are confusing. The sum bound comes from a calculation which is not shown and is of questionable value since it is not used anywhere in the following text. Furthermore, the values of A_L (hard-limiter voltage gain) and $\Delta\omega$ are not indicated anywhere. Spectrum $S_{N_2}(f)$ has been plotted for some value of $\Delta\omega$, but the sum of $S_{N_1}(f) + S_{N_2}(f)$ does not match the sum spectrum. The purpose of the overall argument is to substitute (or upper bound) the sum of noises

$$\frac{\sqrt{2}\,A_L}{\sqrt{\pi}\,\sigma} e^{-\rho_i/2} I_0\left(\frac{\rho_i}{2}\right) \tilde{n}_1(t) + \frac{2\sqrt{2}\,A_L}{\sqrt{\pi}\,\sigma} e^{-\rho_i/2} I_1\left(\frac{\rho_i}{2}\right) \tilde{n}_1(t) \sin(2\Delta\omega t + 2\theta)$$

with a single noise process $\tilde{n}_1(t)$ with an appropriate gain. The simplest way to do it would be to neglect $\sin(\cdot)$ since $|\sin(\cdot)| \leq 1$, then upper bound the sum as

$$\frac{\sqrt{2}\,A_L}{\sqrt{\pi}\,\sigma} e^{-\rho_i/2} I_0\left(\frac{\rho_i}{2}\right) \tilde{n}_1(t) \left[1 + \frac{I_1\left(\frac{\rho_i}{2}\right)}{I_0\left(\frac{\rho_i}{2}\right)}\right]$$

Then, for the range of ρ_i of interest, substitute the ratio $(I_i(\cdot))/I_0(\cdot)$ with an appropriate number of the order of 0.2 - 0.5. Instead, the analysis uses the factor $\sqrt{1.2}$ without further justification. Also, the author states that the resulting noise is essentially flat up to 30 kHz. That is obviously a pessimistic assumption since $\tilde{n}_1(t)$ is simple white bandpass noise filtered by LPF_1, which is a one-pole filter with cut-off frequency of 25 kHz. However, this is not a bad assumption from the point of view that it upper bounds the noise contribution and simplifies the following analysis.

We should point out the following: In the numerical results, it seems that the author uses the value $\Delta f = 0$ since he is interested in the case where the discriminator is centered exactly at $f_c + f_{sc}$. If that

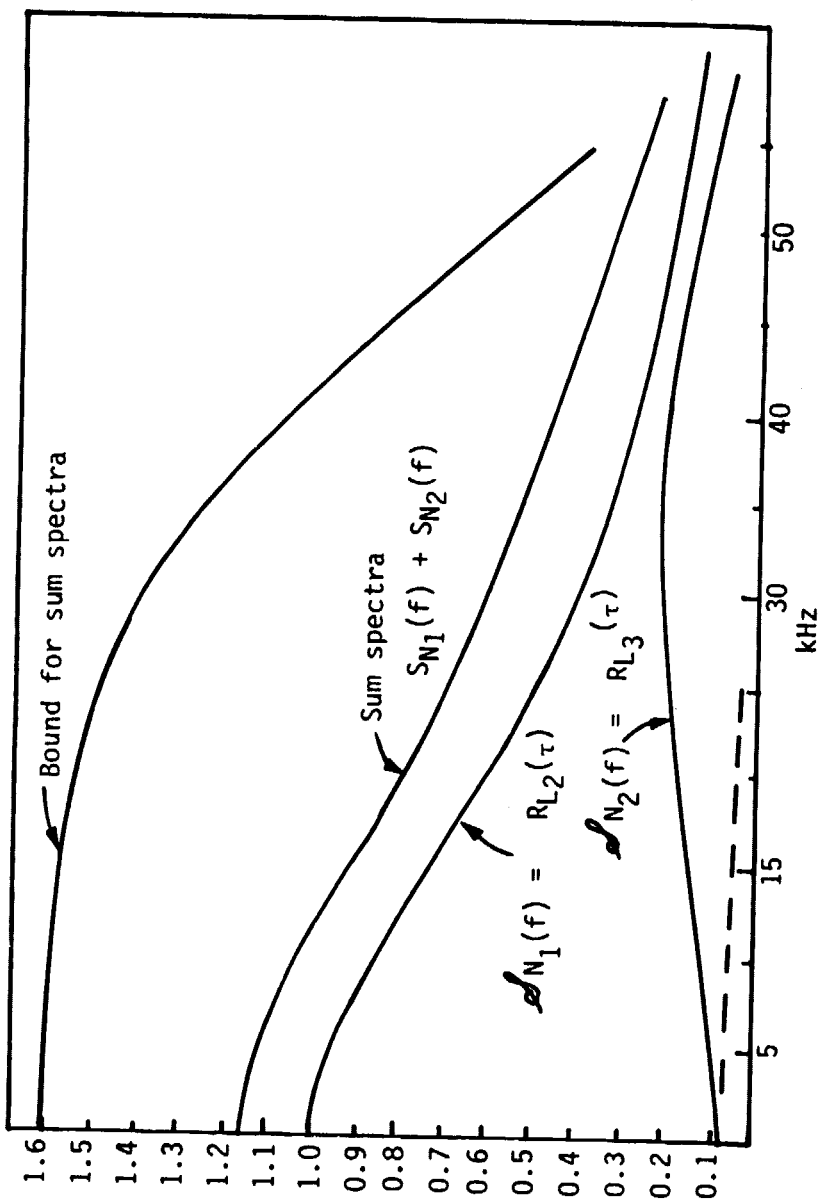

Figure 5. Individual, Composite and Upper-Bound Noise Spectra

is indeed the case (and there is no contrary evidence since the value of Δf does not appear anywhere), all the calculations for $S_{e_3}(0)$ and $S_{e_2}(0)$ are useless becuase they will be zero for $\Delta f = 0$ ((68) and (70)).

In a very heuristic coupling of transient to steady-state concepts, the author models a time-varying input to LPF_3, as shown in Figure 6. The signal level at the output of LPF_3 is calculated based on that input and, from that, the resulting probabilities are calculated. Therefore, such an assumption really affects the overall conclusions of the analysis. This statement is made in light of our lack of faith in using steady-state analysis techniques to calculate the performance of essentially time-varying phenomena. However, an exact assessment of the appropriateness of this assumption is beyond the scope of this review.

For the case of only two signals and noise into a hard limiter, as is the case here, the results of Jones [4] will yield a more accurate answer than Shaft's [5] expression used by the author.

Thus, using Jones' results, we have the carrier and subcarrier components, respectively given by

$$b_{010} = \frac{1}{\pi}\left(\frac{S_1}{N}\right)^{1/2} \sum_{i=0}^{\infty} \frac{(-1)^i\left(\frac{S_1}{N}\right)^i}{i!(i+1)!}\,\Gamma\left(i+\tfrac{1}{2}\right)\,{}_2F_1\left(-i,-i,-1;1;\frac{S_2}{S_1}\right)$$

and

$$b_{001} = \frac{1}{\pi}\left(\frac{S_2}{N}\right)^{1/2} \sum_{i=0}^{\infty} \frac{(-1)^i\left(\frac{S_1}{N}\right)^i}{(i!)^2}\,\Gamma\left(i+\tfrac{1}{2}\right)\,{}_2F_1\left(-i;-i;2;\frac{S_2}{S_1}\right)$$

where

$$S_1 = \frac{A_1^2}{2}\;; \quad S_2 = \frac{A_2^2}{2}\;; \quad N = \sigma^2.$$

We also note that the author's expression for the discriminator dynamic DC output voltage ((95))

$$S = \frac{8\alpha_c^2 A_L^2(75)}{\pi^2}\,\tau(2\pi)\left(16 \times 10^3\right)$$

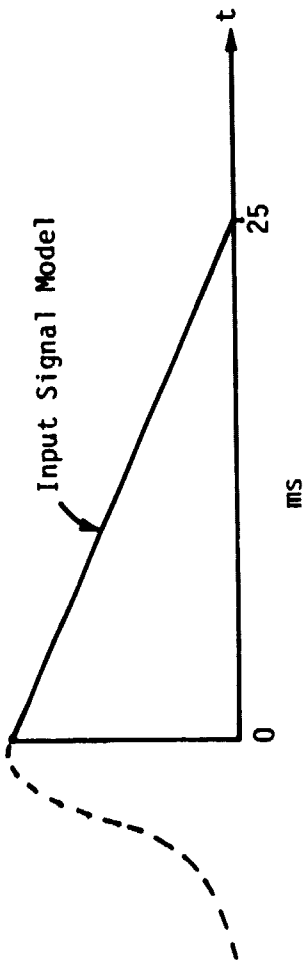

Figure 6. Model of LPF_3 Input Signal Due to Subcarrier

is calculated for $\Delta\omega = 0$; in which case, the second term in his expression for the noise variance

$$\sigma^2 = 3.9 A_L^2 f_0^3 N_0^2 e^{-2\rho} I_0^4\left(\frac{\rho}{2}\right) 2B_{LP} + \frac{76.8\, N_0 \alpha A_L^4 \tau^2}{\pi\sigma^2} e^{-\rho} I_0^2\left(\frac{\rho}{2}\right) \times \frac{(\Delta f)^2 |H_2(\Delta f)|^2}{\left[1 + \left(\frac{\Delta f}{f_0}\right)^4\right]} 2B_{LP}$$

should be zero. Finally, the rationale for the selection of the threshold as $T_h = 1/2\ S$ is not provided.

In summary, we have found some minor flaws in the author's analysis; we also question the appropriateness of using steady-state analytical techniques to analyze time-varying phenomena. However, we do not believe that the minor flaws significantly change the conclusions reached by the author, nor do we have any alternate analytical techniques to suggest. This type of system is difficult to analyze, and the author's efforts probably represent the best that can be done in a reasonable amount of time and at a reasonable cost.

4.0 CDR ACTIVITY

As part of its contractual activity, Axiomatix attended the STDN/TDRS CDR. There were 21 action items and 26 RID's. The action items and RID's primarily concerned the lack of test data to establish the communication performance of the transponder over the link. Tables 2 and 3 present descriptions of the key action items and RID's, respectively. It should be noted that the action items and RID's correspond in most cases to the areas of analysis that Axiomatix is engaged in and documented in Section 3 of this report. Action items that addressed new areas were AI-5, AI-9, AI-10 and AI-21. These new areas were scheduled into the Axiomatix analysis effort but, due to cancellation of the STDN/TDRS transponder effort, were not completed.

Table 2. Key IUS TDRS/STDN Transponder CDR Action Item Descriptions

Item	Title	Description
AI-2	TDRS Command Detection Test Data	Command detection performance needs to be tested over temperature range
AI-3	TDRS Acquisition and Tracking Test Data	Testing of acquisition and tracking of a TDRS signal with ±70 Hz/s doppler rates with a dynamic phase error of < 15° peak.
AI-4	Performance Evaluation with Integrated Tests	The test data presented at the CDR did not include the SSP integrated with the receiver.
AI-5	STE Carrier-Interrupt Time Discrepancy	The transponder, as built, has a 21-ms carrier interrupt time but the allowed carrier drop-out time is 43 ms.
AI-8	Enumeration of Performance Degradations	The performance degradations due to TDRSS user constraint noncompliance needs to be determined.
AI-9	Downconverter #1 In-Band Spurs	In-band spurs are listed as less than -80 dBm, but the requirement is for -100 dBm.
AI-10	Demodulator AGC Worst-Case Analysis	AGC gain is shown to be deficient at end-of-life.
AI-11	Demodulator 2 Spurious Output	The requirement for spurious output is > 136 dBm but the capability is only > 90 dBm. Also, linearity is only 13% rather than 10%
AI-12	RF Filter Description	No data is given for the new preselector and image filters.
AI-21	Decoder Activate/Deactivate Time Constant	There is a defined requirement for the 90% probability decoder deactivate level.

Table 3. Key IUS DRS/STDN Transponder RID Descriptions

Item	Title	Description
RID-2	QPSK Modulator Data Rate	The QPSK modulator must handle the 3-Mchips/second PN rate, but the test data shows a capability for only 2 Mbps.
RID-12	Carrier-Suppression Discrepancy	The test data shows only 27 dB of carrier suppression rather than the required $\geq$ 30 dB.
RID-14	Transmitter Output Power Discrepancy	The test data shows that the output power is less than the required 2.5 W at 160°F when the voltages are at low tolerances.
RID-15	Static Phase Error	Analysis shows that the static phase error may exceed the required $\leq \pm 5°$ in the tracking range of ±100 kHz.
RID-22	Telemetry Data/Clock Skew	The transponder is required to handle data/skew from 250 - 3.5 μs, but the CDR data shows only 50 - 1.9 μs.
RID-23	Receiver Phase Noise Discrepancy	The phase noise in the data bandwidth is required to be less than 3° RMS, but the only data is for less than 15° RMS during vibration.
RID-24	Biphase-L Waveform Symmetry Deficiency	The transmitter is required to reformat the input telemetry so that a waveform symmetry equal to or better than 2% is achieved. The data package states that the output symmetry will be whatever the clock input provides.

5.0 SUMMARY AND CONCLUSIONS

The analyses, reviews and investigations conducted by Axiomatix prior to cancellation of the TRW IUS STDN/TDRS transponder effort uncovered no basic reasons to believe that the transponder would not work satisfactorily with the Orbiter. However, Axiomatix did uncover several minor flaws in some of the analyses performed by TRW. It is doubtful that these flaws would significantly change the conclusion stated above. Had the effort continued, however, Axiomatix would have refined or reanalyzed the areas in question. Furthermore, where some of the analyses for performance in noise were very approximate by necessity, Axiomatix would have conducted computer simulations to verify parameter values and performance.

As a result of its participation in the IUS STDN/TDRS transponder CDR, Axiomatix undertook several new analyses. Due to cancellation of the transponder effort, however, only several of these were completed. These are documented in Section 3 of this final report.

REFERENCES

1. M. K. Simon and W. K. Alem, "Tracking Performance of Unbalanced QPSK Demodulators: Part I--Biphase Costas Loop with Passive Arm Filters," IEEE Transactions on Communications, Vol. COM-26, No. 8, August 1978, pp 1147-1156.

2. M. K. Simon and J. C. Springett, "The Theory, Design and Operation of the Suppressed Carrier Data-Aided Tracking Receiver," JPL Technical Report #32-1583, June 15, 1973.

3. A. Blanchard, Phase-Locked Loops: Application to Coherent Receiver Design, J. Wiley and Sons, 1976, Chapter 11.

4. P. Shaft, "Limiting of Several Signals and Its Effect on Communication System Performance," IEEE Transactions on Communications Technology, Vol. COM-13, No. 4, December 1965.